arXiv:1405.0840v1 [astro-ph.EP] 5 May 2014

Not to appear in Nonlearned J., 45.

# Interstellar Simulations Using A Unified Microscopic-Macroscopic Monte Carlo Model with a full Gas-Grain Network including Bulk Diffusion in Ice Mantles

Qiang Chang

*Department of Chemistry, University of Virginia, Charlottesville, VA 22904 USA*

*Xinjiang Astronomical Observatory, Chinese Academy of Sciences, 150 Science 1-Street, Urumqi 830011, PR China*

*Key Laboratory of Radio Astronomy, Chinese Academy of Sciences, 2 West Beijing Road, Nanjing 210008, PR China*

Eric Herbst

*Departments of Chemistry, Astronomy and Physics, University of Virginia, Charlottesville, VA 22904 USA*

## ABSTRACT

We have designed an improved algorithm that enables us to simulate the chemistry of cold dense interstellar clouds with a full gas-grain reaction network. The chemistry is treated by a unified microscopic-macroscopic Monte Carlo approach that includes photon penetration and bulk diffusion. To determine the significance of these two processes, we simulate the chemistry with three different models. In Model 1, we use an exponential treatment to follow how photons penetrate and photodissociate ice species throughout the grain mantle. Moreover, the products of photodissociation are allowed to diffuse via bulk diffusion and react within the ice mantle. Model 2 is similar to Model 1 but with a slower bulk diffusion rate. A reference Model 0, which only allows photodissociation reactions to occur on the top two layers, is also simulated. Photodesorption is assumed to occur from the top two layers in all three models. We found that the abundances of major stable species in grain mantles do not differ much among these three models, and the results of our simulation for the abundances of these species agree well with observations. Likewise, the abundances of gas-phase species in the three models do not vary. However, the abundances of radicals in grain mantles can differ by up to two orders of magnitude depending upon the degree of photon penetration and the bulk diffusion of photodissociation products. We also found that complex molecules can be formed at temperatures as low as 10 K in all three models.

*Subject headings:* ISM: clouds, ISM: molecules, ISM: molecular processes

## 1. Introduction

In cold dense regions of the ISM, molecules are found in both the gaseous and solid phases. Most species including the most abundant one, $H_2$, are found only in the gas phase. Some species are found to have appreciable abundances in the layers of ice mantles, which cover interstellar grains with possibly more than 100 monolayers of ice in cold dense sources. The most abundant species in the ice mantle is water, the fractional abundance of which with respect to $H_2$ is about $5 \times 10^{-5}$ (Gibb et al. 2004; Pontoppidan et al. 2004; Boogert & Ehrenfreund 2004; Öberg et al. 2011a). The next most abundant species are carbon dioxide and carbon monoxide, with abundances 10-50 percent that of water (Öberg et al. 2011a). Methane, methanol and ammonia possess smaller abundances in the range 1-10 percent of water (Öberg et al. 2011a). Moreover, there might also be small amounts of other stable molecules such as $H_2O_2$, the upper limit of which has been investigated recently (Smith et al. 2011). Some species in the ice mantle, such as carbon monoxide, are formed initially in the gas phase and then accrete onto dust grains while most species are formed from simpler species on the grain surfaces and possibly inside the grain mantles. For example, only a small abundance of methanol can be produced in the gas phase; its dominant mode of production is hydrogenation of CO on grain surfaces via reactions with atomic hydrogen, followed by non-thermal desorption (Watanabe & Kouchi 2002). More complex organic molecules (COMs) such as methyl formate are also believed to be formed on dust grain surfaces via radical-radical reactions during the early stages of a later warm-up phase and then released into the gas (Garrod & Herbst 2006). Such COMs have recently been detected in the gas-phase of cold dense clouds (Bacmann et al. 2012); the details of their formation in these regions are currently not fully understood, but involve both non-thermal desorption of simpler precursor species such as methanol from the grain surface and additional gas-phase reactions (Vasyunin & Herbst 2013a).

The treatment of surface chemical processes on small interstellar grains involves a number of difficulties. Pickles & Williams (1977) and Hasegawa et al. (1992) modeled the surface chemistry in the same way as the approach for gas phase chemistry, via coupled chemical kinetic differential equations. The approach is relatively easy to implement and computationally efficient, thus it is still widely used in gas-grain astrochemical modeling, with the additional approximation that all species in all monolayers of the ice are treated in the same manner. However, this approach has at least three major problems. The first occurs when the average number of reactive species such as atomic hydrogen on grain surfaces is less than one, and significant errors may occur unless the discrete numbers of species and their fluctuations are treated in some manner (Tielens & Charnley 1997; Caselli et al. 1998; Herbst & Shematovich 2003; Lipshtat & Biham 2003). A number of approaches have been suggested to solve this problem. In order of increasing computational complexity, these include the modified rate treatment (Caselli et al. 1998; Garrod 2008), the moment equation approach (Lipshtat & Biham 2003), the chemical master equation approach (Biham et al. 2001; Green et al. 2001), macroscopic Monte Carlo simulations (Charnley 1998), and microscopic Monte Carlo simulations (Chang et al. 2005). Although all of these approaches have been applied to simulate the grain mantle chemistry with either a full surface reaction network or at least more than 10 reactions on grain surfaces (Garrod 2008; Du & Parise 2011; Stantcheva & Herbst 2004;

Vasyunin et al. 2009; Charnley & Rodgers 2009; Chang & Herbst 2012), the computational cost becomes more expensive as the approach becomes more rigorous. The second problem was first considered by Hasegawa & Herbst (1993), who argued that only species on the top layer of a grain mantle will react with each other, so that the bulk layers underneath this layer should remain chemically inert as an ice mantle gradually forms. This approach, now referred to as a three-phase model (top layer, bulk, gas) was virtually ignored for some time after its initial suggestion. Separating species in the bulk from those on the top layer allows abundant and somewhat reactive species such CO or $H_2CO$ or even some very reactive radicals to remain non-reactive in the ice bulk for a long period of time.

Despite the fact that the microscopic Monte Carlo method can account for the non-reactivity of bulk species due to its spatial resolution of species (Chang et al. 2007; Chang & Herbst 2012), different simulation approaches with less computational cost, but which typically do not have the same degree of spatial resolution capability, have also been applied to the problem recently (Garrod & Pauly 2011; Taquet et al. 2012; Vasyunin & Herbst 2013b) . The third problem with the conventional rate-equation method is that the same species on the outermost layer may have different binding energies and diffusion barriers on grain surfaces because of surface roughness, chemisorption, or porosity (Cuppen & Herbst 2005). When reactive species are very volatile, modeling binding sites on a surface as uniform indistinguishable sites can result in large errors because stronger binding sites can help some species to be stabilized on grains until higher temperatures are reached, thus significantly changing the chemical kinetics. The formation of $H_2$ from two atoms is an example where stronger binding sites help to increase $H_2$ formation at higher temperatures when all of the atomic hydrogen on grain surfaces would otherwise sublime back to the gas before combining to form $H_2$ (Cuppen & Herbst 2005; Chang et al. 2005). This problem has been solved by improvements in the conventional rate equation approach (Taquet et al. 2012) or more rigorous microscopic Monte Carlo simulations (Cuppen & Herbst 2005; Chang et al. 2005).

It is clearly true that in order for more accurate astrochemical modeling of ice mantles, any chemical kinetics that occurs in the bulk should be different from that on the top layer, or top several layers of a rough surface. However, it is not as true to treat the bulk as completely inert for several reasons. First of all, volatile species may gradually diffuse out of the mantle and then sublime into the gas phase. This effect has been studied by a rate equation approach with the so-called modified three phase model (Fayolle et al. 2011). In this model, species are able to swap positions with other species in the bulk so that they are mobile. Secondly, recent calculations show that the probability of UV photons to be absorbed by one monolayer of water ice is about 0.7% (Andersson & van Dishoeck 2008). Thus, UV photons can easily penetrate through as much as 150 monolayers of species of water ice in grain mantles and photodissociate species within these monolayers. So species within the bulk are only partially shielded from UV radiation and those more deeply buried within the bulk are less likely to undergo photodissociation. Moreover, the products of photodissociation on the surface and those within the bulk were found to behave very differently (Andersson & van Dishoeck 2008). In particular, the photodissociated species within the bulk were found to diffuse and recombine within the bulk while a large fraction of those

on the surface were found to directly sublime. Recent photodissociation laboratory experiments also qualitatively verify that species photodissociated from bulk water ice can diffuse and then recombine (Öberg et al 2009a).

Motivated by our recent success in unifying a microscopic Monte Carlo simulation for grain chemistry with a macroscopic Monte Carlo simulation for the gas phase (Chang & Herbst 2012), we modified our microscopic Monte Carlo method for surface chemical reactions in order to include reactions and diffusion within the bulk. Moreover, for the first time, we included about 300 surface reactions in the surface reaction network, a large number which is feasible because of our improved simulation algorithm. Photodissociation reactions are also included and the products of photodissociation are allowed to diffuse within the bulk ice mantle. Another recent attempt has been made to include bulk diffusion in an interstellar model. In this attempt, a three-phase model of gas-grain chemistry was utilized with modified rate kinetics to study the formation of glycine and other COMs during the formation of a hot core at 200 K (Garrod 2013a). Here, photodissociation was assumed to occur at equal rates in all layers, while swapping was assumed to be the mechanism for bulk diffusion. Swapping, however, may not be the major mechanism for bulk diffusion at low temperatures because of possibly large barriers against the process. Not surprisingly, Garrod (2013a) found that bulk diffusion is not important for the formation of the ice mantle in the early, low temperature, phase of the calculation.

The remainder of this paper is organized as follows. Our bulk and surface model, reaction network, microscopic-macroscopic Monte Carlo approach, and its application to surface and bulk kinetics are described in the next section. We present our simulation results for cold dense interstellar clouds in Section 3. In Section 4, we compare these results with those of other models and observational results. Finally, our conclusions and a discussion appear in Section 5.

## 2. Physical Model and Monte Carlo Methods

### 2.1. Surface and Bulk Model

There are two mechanisms for bulk diffusion: substitutional diffusion and interstitial diffusion, although motion in internal pores can possibly be considered a third (Kalvans & Shmeld 2013). The bulk diffusion mechanism used in previous models can be classified as substitutional diffusion (Garrod 2013a; Fayolle et al. 2011), in which pairs of bulk species have to replace each other in order to diffuse. Interstitial diffusion, which refers to diffusion involving sites in between normal sites of the normal lattice structure, can be energetically more favorable because species in interstitial sites are generally less strongly bound to other species and there is no additional barrier due to swapping in order to diffuse. The diffusion of photodissociated species in the molecular dynamics simulation of Andersson & van Dishoeck (2008) can be classified as interstitial in nature. In this work, we focus on interstitial diffusion because our model is for temperatures below 20 K; thus, substitutional diffusion is not the major mechanism because of its high barrier. On the other hand, because atomic H is found to be able to react with species in the top four monolayers of the ice

mantle by substitutional diffusion (Cuppen et al. 2009), we include substitutional diffusion in our simulations using a simplified approach as explained later.

To include interstitial diffusion and bulk reactions during the growth of an ice mantle, we modified our procedure for microscopic Monte Carlo simulation with a model that simulates impurity diffusion in semiconductors (Akiyama et al. 1987). As in our earlier work (Chang & Herbst 2012), grains are assumed to be uniform in size with radius $r_{\rm d} = 0.1\mu$m. We start from a bare flat surface where the desorption energy might be different from that on flat water ice; however, because the initial desorption energy does not affect our results (Chang et al. 2007), we still assume that it is the same as that on flat ice. Using a density of regular sites obtained from experiments on high-density ice of $1 \times 10^{15}$ cm$^{-3}$ (Jenniskens et al 1995), there are about $10^6$ regular sites on each grain. Based on our microscopic Monte Carlo simulation of $H_2$ formation (Chang et al. 2005), a flat surface with $10^4$ sites is large enough to avoid a finite size effect while an inhomogeneous (rough) surface can be much smaller to avoid the effect because diffusing species such as H can be trapped on the sites with stronger binding strength and so lie in smaller clusters. A qualitative analysis of sites visited by species on grain surfaces shows that increasing the chemical complexity does not increase the minimum surface area needed to avoid a finite size effect. The more complex species, the greater the chance that traveling H atoms will react within a smaller cluster of sites. So we are able to use a surface, which is initially flat and then becomes rough as time evolves, with only $10^4$ sites, which constitute1% of the whole surface area in our simulation. Based on our earlier work (Chang & Herbst 2012), 1% of gas phase species around one dust particle is also enough to avoid an analogous finite size effect in the gas phase. We put these $10^4$ sites on a square lattice with dimension $200 \times 200$. Nodes in the lattice that have both even numbered x and y coordinates represent real binding sites on the grain surface, which we term "normal." Each normal site has six nearest neighbor sites, four in the same layer and two in upper and lower layers respectively. "Normal" species, which are located on normal sites, can only move horizontally from one normal site to another one by moving two steps, over a potential that includes an intermediate site, which cannot be occupied. Nodes that have both odd numbered x and y coordinates represent interstitial sites, which are also surrounded by six nearest neighbor sites, four of which lie in the same layer. Nodes that have an even numbered and an odd numbered coordinate are forbidden to be occupied at any time.

The horizontal structure of a monolayer is shown in Panels A and B of Figure 1. In these panels, the blue squares represent normal sites, which can only be occupied by normal species, while the yellow squares represent interstitial sites, which can only be occupied by interstitial species. The white squares cannot be occupied. What differentiates Panels A and B are the allowed processes on the surface, or topmost, monolayer (Panel A) and any bulk ice monolayer (Panel B). On the surface, only normal species are allowed. They hop from one blue square to another, accrete onto blue squares, desorb into the gas from blue squares, and undergo photodissociation from blue squares. The lighter of the two photodissociation products moves to a nearest neighbor normal site while the heavier of the two remains in the site occupied by the parent. Finally, chemical reactions can occur when two species are in the same normal site. These processes mimic the

surface processes included in earlier treatments. Motion in bulk layers involves the interstitial sites: like normal species on the surface, interstitial species in the bulk can undergo horizontal hopping to nearest neighbor interstitial sites and undergo reaction if two species wind up on the same interstitial site. Interstitial species, however, can also undergo vertical hopping to upper and lower levels, and react if two end up in the same site. Conversion between normal and interstitial species occurs via several processes. Normal species in bulk layers can undergo photodissociation; the lighter product ends up in an interstitial site. Interstitial species become normal species when they move to the top layer, where there are no interstitial sites. Essentially, instead of remaining in an interstitial site on the topmost layer, the hopping interstitial species is placed in a neighboring normal site. There is also a reactive process in which a species in an interstitial site reacts with one in a nearest neighbor normal site, with the product to be put in the normal site if there is only one product. If there is more than one product, that with the largest diffusion barrier is put in the normal site and all other products put in neighbor interstitial sites.

In order to simulate the chemical kinetics on and in grain mantles, four parameters have to be specified. The first is the diffusion barrier on the top layer, $E_{\rm b}$, which determines how fast normal species hop from one normal site to another. The hopping rate is calculated as $b_1 = \nu \exp(-E_b/T)$ where $\nu$, the second parameter, is the trial frequency and $T$ is the grain temperature. The trial frequency is set to be $2 \times 10^{11}$ s$^{-1}$ which is lower than the standard value $10^{12}$ s$^{-1}$. We use the lower value because the temperature dependent reaction barriers of H + CO and H + $H_2CO$ are fitted with the lower trial frequency (Fuchs et al. 2009). The third is the desorption, or sublimation, energy, $E_{\rm D}$, which determines how rapidly normal species are thermally desorbed. The rate for sublimation is given by $b_2 = \nu \exp(-E_D/T)$. The last parameter is the diffusion barrier within the bulk, $E_{b2}$, which determines how rapidly interstitial species diffuse. The interstitial diffusion rate is given by $b_3 = \nu \exp(-E_{b2}/T)$. We choose the relation, $E_{b0} = 0.5E_{D0}$ for a flat icy surface (Garrod & Herbst 2006), with desorption energies for assorted species taken from Garrod & Herbst (2006). However, the real surface may be rough, so normal species on the top layers may form lateral bonds with neighboring normal species. The actual diffusion barrier for normal species on these top layers is given by the expression $E_{bi} = E_{b0i} + nE_{Li}$ where $E_{Li} = 0.1E_{D0i}$ is the strength of lateral bonds formed between normal species and water (the dominant ice), $i$ refers to a particular species, and $n$ is the number of lateral bonds. The strength of lateral bonds is not well known and has been chosen to ensure sufficient mobility for species and yet be strong enough to form $H_2$ efficiently (Cuppen & Herbst 2005). We only consider lateral bonds between normal species because the bond formed by normal species and interstitial species is weaker and also interstitial species will become normal species when they diffuse to the top of the grain mantle, so there are very few interstitial species on the top few layers. Similarly, we have $E_{Di} = E_{D0i} + nE_{Li}$, which only refers to the normal species. For a detailed explanation of how we calculate $E_{\rm b}$ and $E_{\rm D}$, we refer to our earlier paper (Chang & Herbst 2012). In fact, if we ignore interstitial sites and interstitial species, the bulk and surface models here are the same as what we used before (Chang & Herbst 2012). In the work by Garrod (2013a), which focuses on substitutional bulk diffusion, the bulk diffusion barrier is chosen to be $0.7E_D$. Here we focus on interstitial bulk diffusion, which is a different physical process and highly uncertain. However, because bulk diffusion is normally slower

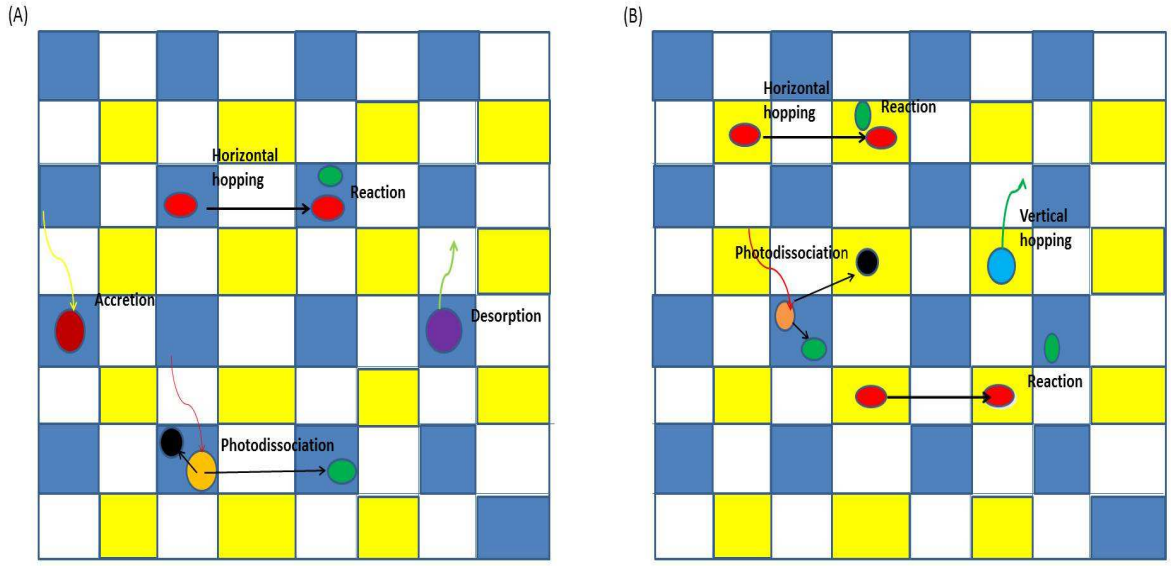


Fig. 1.— Major processes on grain surfaces. Blue sites are normal sites, occupied by normal species, while yellow sites are interstitial sites, occupied by interstitial species, and white sites cannot be occupied. Panel (A) shows the topmost layer, while Panel (B) shows an inner (bulk) layer. The differing processes that occur in the topmost layer and the bulk layers are discussed in detail in the text. Note that although Panel A shows yellow squares, no interstitial sites exist on the topmost layer.

than diffusion on the surface, we choose the barrier to be $E_{b2i} = 0.7E_{D0i}$ or $E_{b2i} = E_{D0i}$. The first value will ensure that interstitial species will diffuse more slowly than normal species do on the top layers while small interstitial species such as H can still diffuse rapidly enough to lead to reactions even at 10 K. The second value essentially allows only the weakly bound atomic H to diffuse within the bulk. Even atomic H cannot diffuse within the bulk if we assume a higher value of $E_{b2}$, so it is not interesting to set $E_{b2}$ at still higher levels.

### 2.2. Gas-grain Model

The physical conditions in our simulation pertain to cold dense cores. The chosen temperature is 10 K or 15 K and the density of H nuclei, $n_{\rm H}$, is fixed at $2 \times 10^4$ cm$^{-3}$. The cosmic-ray ionization rate is set at $\zeta_{H_2} = 1.3 \times 10^{-17}$ s$^{-1}$. Reactions, rate coefficients, and species are taken from Vasyunin & Herbst (2013b), with some exceptions. As noted previously by other authors (Garrod et al. 2009), the sparse nature of the surface network can lead to catalytic pathways, which can eat up much of the atomic hydrogen, so that H atoms will be converted to $H_2$ and so hinder the formation of species such as water and methanol. The two reactions below are excellent examples:

$$\begin{array}{ccccccc} \mathrm{H} & + & \mathrm{H_2O_2} & \rightarrow & \mathrm{O_2H} & + & \mathrm{H_2}, \\ \mathrm{H} & + & \mathrm{HNO} & \rightarrow & \mathrm{NO} & + & \mathrm{H_2}. \end{array} \quad (1)$$

Although these reactions have barriers of 1900 K and 500 K respectively, they appear to start catalytic cycles in which the products associate with H atoms to re-form the reactants unless there are competitive pathways, not considered in our network. It should be noted that the second reaction does not appear to be important in laboratory experiments leading to the formation of $NH_2OH$ on ice (Congiu et al. 2012), while the first reaction must compete with the more standard products $H_2O$ + OH. In addition, as in Vasyunin & Herbst (2013b), we do not allow any $H_2$ to remain on grains and so include no surface reactions involving $H_2$. We neglect surface $H_2$ because the high abundance of gaseous $H_2$ and the low desorption energy of molecular hydrogen on grain surfaces make Monte Carlo simulations that include rapid molecular hydrogen accretion and desorption not feasible currently (Vasyunin & Herbst 2013a).

Some other granular reactions have reaction barriers and we adopt the values in Vasyunin & Herbst (2013b) except for the barriers pertaining to H + CO and H + $H_2CO$, which are temperature dependent based on recent laboratory measurements (Fuchs et al. 2009). The reaction barrier at 10 K is found by assuming that reaction rates for CO + H and $H_2CO$ + H at 10 K are the same as that at 12 K. In total, we include 4402 gas phase reactions other than accretion and 459 gas phase species. The number of surface/mantle reactions other than photodissociation and desorption is 238 and there are 193 surface species. The initial gas-phase abundances are listed in Table 1, and are based on a particular assumption of low-metal abundances (Semenov et al. 2010). We assume an initial value for atomic hydrogen based on gas-phase models. The dust-to-gas number ratio is fixed at $10^{-12}$.

Photodissociation and photodesorption are included in our simulations. The far-ultraviolet (FUV) flux, $F_{FUV}$, is given by the expression

$$F_{FUV} = G_0 F_0 e^{-\gamma A v} + G_0^{'} F_0, \tag{2}$$

where $G_0 = 1$ is the external radiation scaling factor, $G_0^{'} = 10^{-4}$ is the scaling factor for cosmic ray induced photons based on the calculation of Shen et al. (2004), and $F_0$ is the standard interstellar radiation field with a value of $10^8$ cm$^{-2}$ s$^{-1}$. The exponential factor $\gamma$ is set at 2 based on the experimental analysis of Öberg et al. (2007). Because the second term on the right-hand side of eq. (2) is much larger than the first term in dense clouds, the rate coefficient for photodissociation of a species $i$, $k_{FUV,i}$, is calculated based on the second term only in our simulation.

When photons hit grain surfaces, one important parameter for photodissociation is the probability that species in each monolayer absorb the photons. However, little is known about the probability of photon absorption per monolayer for different species except water, which was estimated theoretically to be $P_0 = 0.007$ (Andersson & van Dishoeck 2008). To obtain the probability of photon absorption per monolayer for a species $i$, we assume that this probability is proportional to the photodissociation rate on grain surfaces, and that these rates and products are the same as their gas-phase analogs. The probability of photodissociation for a molecule, $i$, per monolayer is proportional to the overall photodissociation rate. For a molecule , i, it is $\sum k_{FUV,mi}$, which is the sum of all rate of product channels $m$. Thus, we can estimate the probability that a species $i$ absorbs FUV photons per monolayer as

$$P_i = P_0 \frac{\sum k_{FUV,mi}}{\sum k_{FUV,m0}}, \tag{3}$$

where $k_{FUV,m0}$ is the photodissociation rate coefficient for water in the m-th product channel (Semenov et al. 2010).

Table 1: Initial Gas Phase Abundances

| Species | Fractional Abundance w.r.t. $n_{\mathrm{H}}$ |
|---|---|
| He | $9.00 \times 10^{-2}$ |
| H | $1 \times 10^{-4}$ |
| $H_2$ | $5 \times 10^{-1}$ |
| $C^+$ | $1.2 \times 10^{-4}$ |
| N | $7.6 \times 10^{-5}$ |
| O | $2.56 \times 10^{-4}$ |
| $S^+$ | $8.0 \times 10^{-8}$ |
| $Si^+$ | $8.0 \times 10^{-9}$ |
| $Na^+$ | $2.0 \times 10^{-9}$ |
| $Mg^+$ | $7.0 \times 10^{-9}$ |
| $Fe^+$ | $3.0 \times 10^{-9}$ |
| $P^+$ | $2.0 \times 10^{-10}$ |
| $Cl^+$ | $1.0 \times 10^{-9}$ |

### 2.3. Monte Carlo Methods

The macroscopic Monte Carlo method for gas phase chemistry here is the same as that used in our previous work (Chang & Herbst 2012; Gibson & Bruck 2000). However, because the modified surface model we use in this work is more complex than that used previously, we have to modify the microscopic Monte Carlo methods. In this subsection, we briefly introduce our microscopic Monte Carlo method then emphasize the modifications needed. A thorough discussion of the unified macroscopic-microscopic approach can be found in Chang & Herbst (2012).

The microscopic Monte Carlo simulation of the movement and reactions of normal species on the grain is essentially the same as used previously (Chang & Herbst 2012). Normal species can hop from one normal site to another by moving two steps with rate $b_1$, and they can sublime into the gas phase with a rate $b_2$. We determine whether a normal species hops or evaporates by comparing $b_1/(b_1+b_2)$ with a random number $W$ that is uniformly distributed between 0 and 1. (Unless stated otherwise, all random numbers defined in this work lie between 0 and 1.) If $W$ is smaller, then the normal species hops, otherwise it evaporates. The waiting time between events is calculated as $\tau = -\frac{\ln Q}{b_1+b_2}$ where $Q$ is another random number. When species accrete onto grain surfaces from the gas phase, they occupy normal sites and become normal species. Chemical reactions happen by three mechanisms. The first is the Langmuir–Hinshelwood mechanism, which occurs when normal species hop to sites where there are reactive species. The second is the Eley-Rideal mechanism, which occurs when species accrete from the gas phase and immediately collide with species in the sites where they land. The last bears the name "Chain" reactions, which we defined in our previous paper (Chang & Herbst 2012). This mechanism occurs when products of a surface reaction can subsequently react with species below them. The most significant example is the production of $CO_2$ at 10 K. We use the competition mechanism to determine whether a reaction with an energy barrier can happen or whether the reactants diffuse away (Herbst & Millar 2008). Binding sites, which are potential minima, are pre-defined in our on-lattice microscopic Monte Carlo simulation, thus all species are assumed to be "point" particles. So, the size of species is not considered. A more rigorous approach, known as the off-lattice microscopic Monte Carlo technique, which calculates the location of potential minima on the fly, can take into account the size of each species on a grain surface (Garrod 2013b). However, it is not our purpose to perform off-lattice microscopic Monte Carlo simulations in this paper.

The movements and reactions by interstitial species represent the newly added part of the current gas-grain model. Interstitial species can only diffuse from one interstitial site to another with diffusion rate $b_3$ within the bulk, where the waiting time for diffusion events is $\tau^{'} = -\frac{\ln X}{b_3}$ with $X$ a random number. An interstitial species has equal probability to diffuse to its six nearest neighboring sites. If the diffusive motion leads to two reactive species in the same interstitial site, a chemical reaction happens. Moreover, whenever an interstitial species comes to a new empty site, or cannot react with a species in the interstitial site, we determine if this interstitial species can react with any of its four nearest neighboring normal species in the same layer. This move is based on the molecular dynamics calculation by Andersson & van Dishoeck (2008), in which photodissociation products can recombine. Thus interstitial species must be able to react with

normal species in our model. If there is more than one neighboring normal species that can react with the interstitial species, we randomly pick one normal species to react. We put the product species with the largest desorption energy in the normal site and all other product species are put into neighboring interstitial sites around the normal site. However, if an interstitial species comes to an already occupied interstitial site and there is no reaction with the interstitial species or neighboring normal species it is a null event, and the interstitial species is returned to its original site. This procedure is undertaken to ensure that an interstitial site is either empty or occupied only by one species. In addition, if an interstitial species randomly comes to an interstitial site with no species right above it (closer to the surface), we allow the interstitial species to continue to move, first to proceed to the empty interstitial site immediately above it and then to a neighboring normal site. This series of moves simulates the process of how volatile species diffuse out of the ice mantle. The process is illustrated by the movement of an interstitial H atom in a matrix of normal water molecules, as depicted in Figure 2.

Photodissociation processes are the only ones that change normal species into interstitial ones. The FUV photon arrival rate onto a grain is calculated as

$$k_{pho} = F_{FUV}\pi r_d^2, \tag{4}$$

where $F_{FUV}$ is the FUV flux as in eq. (2) while the waiting time for an FUV photon arrival is calculated as $\tau^{''} = -\frac{\ln X^{'}}{k_{pho}}$, where $X^{'}$ is a random number. In addition to photodissociation, photodesorption can also occur when FUV photons arrive on grain surfaces. We assume that photodesorption occurs only in the top two monolayers with yields per photon of $Y_{\rm d} = 0.001$ for all species, a value supported by recent laboratory measurements (Öberg et al 2009b; Öberg et al. 2009c). The Monte Carlo simulation of photon arrival events is done in the following manner. First, we randomly pick a normal site where an FUV photon will hit. We ignore photodissociation and photodesorption of interstitial species because they are much less abundant than normal species. For a normal species $i$ on the topmost monolayer, we generate a random number, $Y$. If $Y < Y_{\rm d}$, photodesorption occurs and the normal species desorbs into the gas phase. If $Y > Y_{\rm d}$ and $Y < P_i$ (see eq.(3)), the normal species will be photodissociated. In order to determine the specific channel that photodissociation occurs into, we generate another random number, $Y^{'}$, and compare this number with the branching fractions of products in the specific channels according to the method of Gillespie (1976).

All products of photodissociated species in the topmost monolayer are normal species. If $Y > P_i$, the FUV photon will penetrate through the topmost monolayer and we determine if normal species in the monolayer below the topmost monolayer can be photodesorbed or photodissociated in a similar manner to what we did for normal species in the topmost monolayer. The only difference is that if photodissociation occurs from the second layer, the product with the largest desorption energy will still occupy the normal site while the products with smaller desorption energies will occupy neighboring interstitial sites and become interstitial species if the neighboring normal sites are occupied. If, on the other hand, the neighboring sites are unoccupied, the products will occupy them. If the normal species below the topmost layer can neither be photodissociated

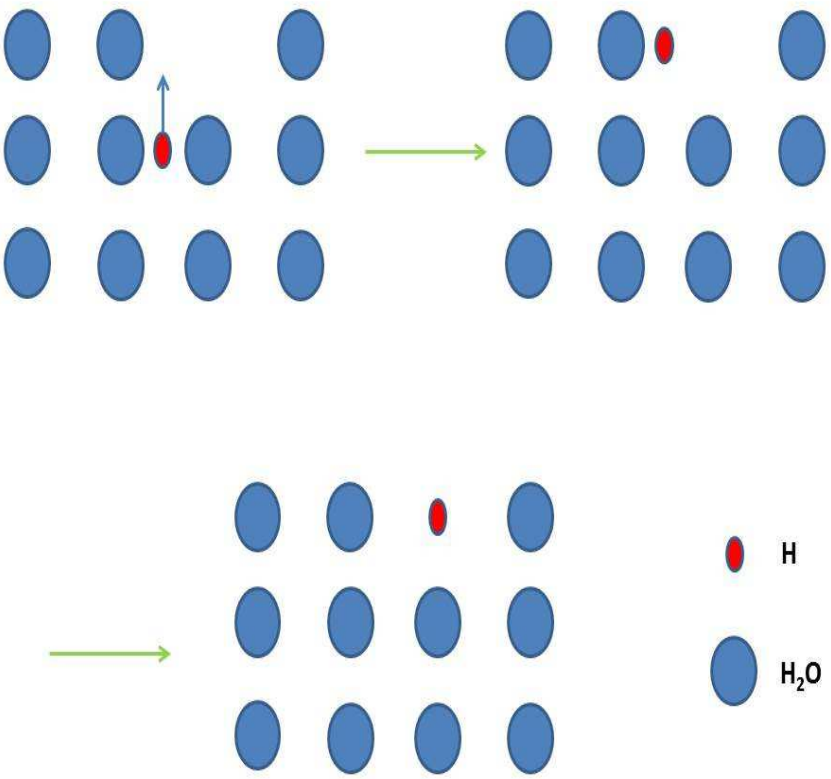


Fig. 2.— An interstitial H atom, shown in red, undergoes a series of moves in which it diffuses out of the bulk. The initial movement upwards occurs randomly with a probability of 1/6. See text.

nor photodesorbed, we move on to the species directly below it, although now we only have to check if it can be photodissociated. The products of the photodissociation of species at this monolayer are treated in the same way as we did for photodissociation of normal species below the topmost monolayer, We continue in this manner until the FUV photon is absorbed or hits the grain base, which is a null event.

The probability that a photon can penetrate through n-1 layers of ice and be absorbed by the n-th layer of ice is

$$P_{pho_n} = P_{i_n} \Pi_{m=1}^{m=n-1} (1 - P_{i_m}). \tag{5}$$

where $i_m$ is the species at the m-th layer on the site where photons hit and we assume the topmost layer to be the first. The exponential nature of the penetration is obvious if the ice mantle is composed of pure water ice, so that

$$P_{pho_n} = P_0 (1 - P_0)^{n-1}. \tag{6}$$

We have run three models of cold dense clouds, each at temperatures of 10 K and 15 K. In Model 1, the barrier for interstitial species to move from one interstitial space to another, $E_{b2}$, is set at $0.7E_{D0}$ (see Section 2.1). Model 2 contains a high barrier $E_{b2} = E_{D0}$. Because we are also interested in how photon penetration affects ice formation on dust grains, we also run a model, labelled Model 0, in which FUV photons can only photodissociate species in the top two monolayers, as occurs for photodesorption in all three models. For Model 0, we also put the products of photodissociation in the monolayer below the topmost monolayer into the topmost monolayer in order not to have any interstitial species in the system, which is comparable to an earlier approach to photodissociation (Vasyunin & Herbst 2013a). Since there are no interstitial species in Model 0, there is no interstitial bulk diffusion although substitutional bulk diffusion in the first 4 monolayers still exists.

To run a Monte Carlo simulation, we must continually determine the event that will occur first and then execute that event. In order to do that for our microscopic simulation, we find the time $t_g$ of the first chemical reaction to occur in the gas phase, the time $t_n$ for the first hopping or evaporation time of normal species in the topmost monolayer and the first time $t_i$ when interstitial species diffuse. We then find the minimum of these times and the photon arrival time $t_p$ to define the overall event to occur first: $t_m = min(t_g, t_n, t_i, t_p)$, and then execute the event. The process repeats itself. To find $t_n$ at each time step, we have to compare up to $L^2$ absolute evaporation or hopping times, where $L^2$ is the total number of normal sites at each layer. Species such as atomic H can hop very quickly, and the time step is very small when fast hopping exists on the grain surface. This problem can make the computational cost very expensive. In order to solve this problem, we have modified our Monte Carlo methods by dividing normal species into three categories based on the diffusion barrier. Atomic H, with the lowest barrier, belongs to category A; atomic O, C, and N, with somewhat higher barriers, belong to category B; and all other species belong to category C. We find the first hopping or evaporation time $t_{nA}, t_{nB}, t_{nC}$ in each of these three categories, separately. We then find the minimum of the three times: $t_n = min(t_{nA}, t_{nB}, t_{nC})$.

If, for example, atomic hydrogen hops or evaporates, we only have to update the absolute time of the first events in category A, which is much faster than comparing all absolute hopping or evaporation times for normal species on the grain surface because there are typically at most a few H atoms present. Thus, although H atoms hop very quickly, the computational cost for each hop is much smaller. We found that this simple modification can reduce the simulation time by a factor of 30 at 10 K. Similarly, we divide interstitial species into three categories and find the first diffusing interstitial species by comparing the absolute time of the first events in each category. This more efficient algorithm is a low-temperature one; as the temperature rises, the distinction among the three classes is reduced.

## 3. Results

We perform our simulations under standard dense cloud physical conditions, as described in section 2.2. Each simulation is run for a time period of $2 \times 10^5$ yr, at which time the abundance of water ice on grain surfaces fits observations. Moreover, the simulated abundances of most gas-phase species typically agree well with observational results at this time. As in our previous paper (Chang & Herbst 2012), which only contained a small number of grain surface reactions, each model simulation was run 4 times with different random seeds and the results we report here are averages of these four simulations. Because our calculated gas-phase abundances during this time interval do not vary much among our three models and previous work, we focus on the ice mantle species. We first report results of the major stable granular species $H_2O$, CO, $CO_2$, $NH_3$, $CH_4$, $H_2CO$, and $CH_3OH$ because these species can be compared with observations. Except for ammonia, these species were discussed in our previous paper (Chang & Herbst 2012). Because radical abundances are sensitive to photon penetration and bulk diffusion, we emphasize the abundances of the radicals OH, $CH_2OH$, and HCO and compare our results with previous work. The radical OH was chosen because it is one product of the photodissociation of the water ice molecule, which is the most abundant species in ice mantles, while $CH_2OH$ and HCO are the reactants that combine to form methyl formate at higher temperatures. We do not differentiate between $CH_2OH$ and $CH_3O$ in our reaction network.

### 3.1. Major species

Figure 3 shows and compares the abundance of major stable species as a function of time at 10 K and 15 K with Model 1 and Model 0 respectively. We do not show results from Model 2 because they are very much like those of Model 1. The abundance of a species is the sum of the species that occupy normal sites and interstitial sites. It is expressed in monolayers; one monolayer of species is equivalent to a fractional abundance of $10^{-6}$ with respect to the density of total H atoms. As can be seen, the abundances of all major surface species increase with time. This increase occurs because although species such as CO may react with H atoms, they cannot continue reacting efficiently after being buried, even if some interstitial species can be formed by photodissociation.

Comparing the results from Model 1 and Model 0, we can see that photon penetration and bulk diffusion (initiated by photodissociation) hardly change the abundance of major stable species, which is not surprising because photodissociation is not a major chemical process in dense clouds. Thus, the fact that species deeply buried in ice mantles can be photodissociated does not change the total abundances of major species significantly. Moreover, as in the gas phase, surface species do not change much when the temperature is increased from 10 K to 15 K. The only difference is that $NH_3$ is the second most abundant species at 10 K while CO is the second most abundant species at 15 K, which can be explained by the fact that the abundance of H atoms decreases at higher temperatures and so cannot hydrogenate nitrogen atoms as efficiently. We summarize the abundances of major stable species for all models at $2 \times 10^5$ yr in Table 2.

Figure 4 shows the fraction of each monolayer occupied by major stable species. We see again that Model 1 and Model 0 results differ very little because photodissociation reactions have minor effects on the abundance of major stable species. Model 2 results are once again not shown because they are very similar to those of Model 1. The temperature difference, on the other hand, can produce a significant difference in the outer layers, because the mobility of species increases exponentially with temperature. Regarding the dependence of abundance on layer, the abundance of water almost stays constant, which shows that water can be efficiently formed on grain surfaces in all models. The surface CO abundance increases at the outer layers when gas phase CO increases. The gasous atomic H abundance almost remains constant in the simulation while gaseous species such as O, which can react with atomic H on grain surfaces without a barrier, decrease, so species such as CO can be more easily hydrogenated at the outer layers. Thus, methanol generally also increases at the outer layers because of the increase in CO and lessened ability of less abundant species such as O to compete for H atoms. The abundance variation of $H_2CO$ is complex because it is an intermediate product of the gradual hydrogenation of CO to methanol. Ammonia also increases slightly in abundance at the outer layers because of the greater availability of H atoms despite the gradual decrease of gas phase N. Carbon dioxide is mainly produced via the chain mechanism between CO and OH (Chang & Herbst 2012), so its abundance increases as the CO abundance increases.

The results concerning the abundances of major species in the ice clearly do not depend much on interstitial sites. Table 3 shows the abundances of the major stable interstitial species in Models 1 and 2 as a percentage of the overall water ice abundance, and one can see immediately that the numbers are all quite small. Overall the abundance of interstitial species is much lower than normal species because photodissociation is the only process that can convert normal species into interstitial species; however, the radiation level in dense clouds is so low that photodissociation reactions occur far less frequently than accretion. In the following detailed discussion of the interstitial abundances, we use $N(i)$ to represent normal species $i$, and $I(i)$ to represent the interstitial species. Interstitial CO can be produced by direct photodissociation such as via N(HNCO) $\rightarrow$ I(CO) + N(NH) or by the association of two interstitial species; e.g., I(O) + I(C) $\rightarrow$ I(CO). We can see that the I(CO) abundance increases as temperature increases in both Model 1 and Model 2. On the other hand, because I(O) and I(C) can hardly move even at 15 K in Model 2, the increase of I(CO) mainly

comes from the increased photodissociation of normal species such as N(HNCO). Species other than I(CO) in Table 3 cannot be produced by direct photodissociation because few photodissociation reactions have them as products. Moreover, even if these molecules appear in the products of photodissociation reactions, since their diffusion barriers are typically larger than other molecules, they still occupy normal sites in our simulation. These interstitial species in Table 3 have to be produced by reactions involving solely interstitial molecules. We can see that as temperature increases, their abundances typically increase with temperature because of the increased mobility of reactive interstitial species. It is also interesting to see that despite the fact that N(CO) can be sufficiently hydrogenated all the way to form N($CH_3OH$) on the topmost layer, it is not easy to hydrogenate I(CO) sufficiently to form I($CH_3OH$) within the bulk although I($H_2CO$) can be produced by gradual hydrogenation of I(CO). These facts suggest that species occupying interstitial sites within the bulk are less likely to be hydrogenated than species occupying normal sites on the topmost layer. Another interesting fact is that I(CO) is the most abundant stable interstitial species instead of water, because CO is a direct product of photodissociation reactions while water molecules are not.

### 3.2. Radicals

Figure 5 shows the abundance (in monolayers) of selected granular radicals as a function of time for Models 0, 1, and 2. First, we compare Models 1 and 0 to determine the influence of photon penetration and bulk diffusion. Contrary to the stable major species, the abundances of radicals in Model 1 are about 1 or 2 orders of magnitude higher than in Model 0 at $2 \times 10^5$ yr, although the abundances of radicals in the three models are similar at earlier times ($< 10^4$ yr) at 10 K. Before the system has evolved through $10^4$ yr, there are fewer than 4 monolayers of ice formed on the grain surface. The H atoms on the mantle surface are able to react with radicals on these monolayers via our H atom swap mechanism, so normal radicals produced before $10^4$ yr are still reactive in all three models. Moreover, interstitial H, which is the only interstitial species that moves at 10 K, can easily diffuse out of the ice mantle when it is very thin, so that interstitial chemistry is not important before $10^4$ yr. So, we cannot see any difference for radicals in the three models at these times. However, when the system has evolved longer, there are enough monolayers of ice covering the grain surface so that radicals produced by photodissociation and deeply buried below top 4 monolayers are no longer able to react with surface H atoms. However, interstitial chemistry becomes more important when it is more difficult for bulk atomic H to diffuse out of the ice mantle. Thus, the difference between these models quickly becomes larger as time evolves. At 15 K, however, because species diffuse more quickly, radicals produced on the topmost layer can easily react with other species before they are deeply buried below the top 4 monolayers of ice. So we can see that there are few radicals produced before $10^4$ yr.

It is also interesting to see where these radicals are located in the ice mantle in Model 1 because the fraction of radicals in interstitial sites can measure the significance of bulk diffusion compared with direct photodissociation to produce interstitial radicals. First consider the radical OH. If it

Table 2: Abundances of Major Stable Mantle Species

| Species | Model 1 10 K | Model 1 15 K | Model 2 10 K | Model 2 15 K | Model 0 10 K | Model 0 15 K |
|---|---|---|---|---|---|---|
| CO | 15.3 | 30.8 | 14.9 | 30.5 | 13.7 | 29.6 |
| $H_2CO$ | 7.7 | 6.3 | 7.4 | 6.1 | 7.7 | 6.1 |
| $CO_2$ | 9.1 | 11.3 | 9.1 | 11.3 | 10.0 | 12.2 |
| $CH_3OH$ | 4.7 | 3.8 | 4.7 | 3.8 | 6.3 | 4.7 |
| $CH_4$ | 11.0 | 5.8 | 11.1 | 5.3 | 13.7 | 6.1 |
| $NH_3$ | 20.9 | 16.1 | 20.9 | 15.9 | 23.2 | 17.2 |
| $H_2O$ | 5.7(-5) | 6.0(-5) | 5.8(-5) | 5.9(-5) | 5.7(-5) | 5.9(-5) |

Note. — The abundances refer to a time of $2 \times 10^5$ yr for Models 0, 1, and 2 at different temperatures. The abundance of total water ice(normal + interstitial) is the fractional abundance with respect to gas-phase $n_{\rm H}$, while the abundances of the other ice components are percentages with respect to the total water ice. a(-b) means a$\times 10^{-b}$.

Table 3: Abundances of Major Stable Mantle Interstitial Species

| Species | Model 1, 10 K | Model 1, 15 K | Model 2, 10 K | Model 2, 15 K |
|---|---|---|---|---|
| CO | 1.3(-1) | 4.5(-1) | 1.2(-1) | 4.6(-1) |
| $H_2CO$ | 1.1(-3) | 2.4(-3) | 9.1(-4) | 2.3(-3) |
| $CO_2$ | 0 | 2.4(-3) | 0 | 4.2(-4) |
| $CH_3OH$ | 0 | 1.0(-3) | 0 | 4.2(-4) |
| $CH_4$ | 2.2(-2) | 3.7(-2) | 1.8(-2) | 1.8(-2) |
| $NH_3$ | 0 | 0 | 0 | 0 |
| $H_2O$ | 1.1(-2) | 6.1(-2) | 8.4(-3) | 9.9(-3) |

Note. — The abundances refer to a time of $2\times 10^5$ yr for Models 1 and 2 at different temperatures. The abundances are percentages with respect to the overall (normal + interstitial) water ice abundance; thus the CO abundance for Model 1 at 10 K is 1.3(-3) of the water abundance. a(-b) means a$\times 10^{-b}$.

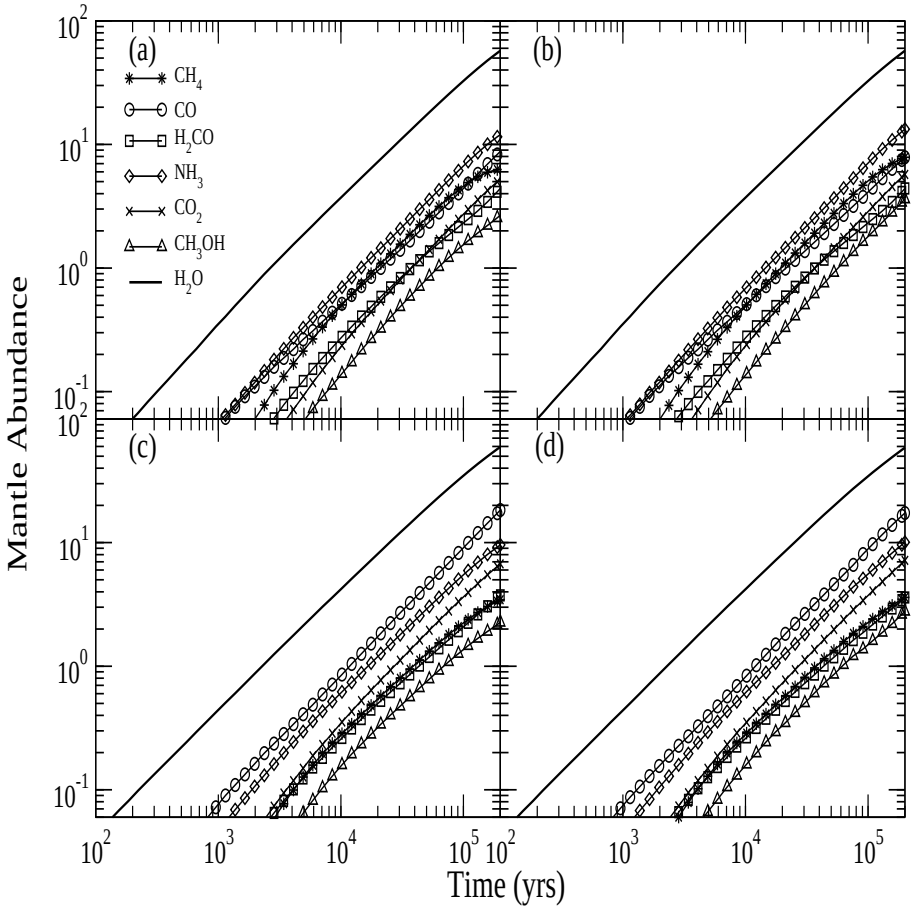


Fig. 3.— The abundances of major stable species in the ice mantle are shown in terms of monolayers as a function of time. Panel (a): $T = 10$ K, Model 1, panel (b): $T = 10$ K, Model 0, panel (c): $T = 15$ K, Model 1, panel (d): $T = 15$ K, Model 0.

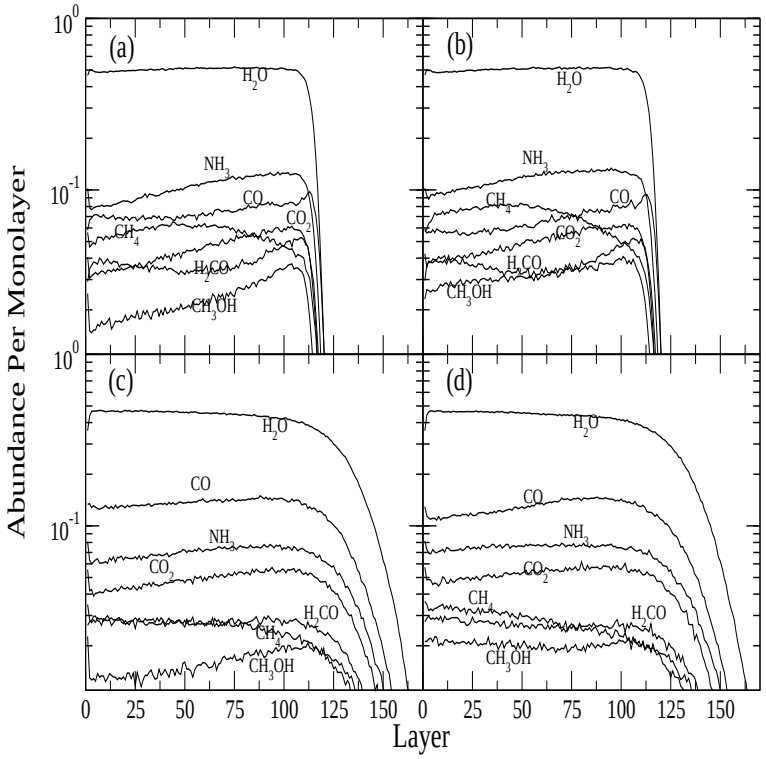


Fig. 4.— The fraction of each monolayer occupied by major stable species in Models 1 and 0 shown as a function of monolayer at the final time of $2 \times 10^5$ yr. Panel (a): $T = 10$ K, Model 1, panel (b): $T = 10$ K, Model 0, panel (c): $T = 15$ K, Model 1, panel (d): $T = 15$ K, Model 0.

formed mainly from the photodissociation of water, it would stay on the normal site while the lighter H atom would go to an interstitial site. Thus, OH in an interstitial site is probably formed just by the association between O and H via bulk diffusion. Now consider the HCO and $CH_2OH$ radicals. If they were formed mainly via photodissociation of the parent species formaldehyde and methanol, they would also remain on normal sites. But, almost all HCO and $CH_2OH$ are hydrogenation products of CO molecules in interstitial sites, the formation mechanism of which has been discussed in detail in the last subsection. Thus, in general, the fraction of radicals in interstitial sites can measure the significance of bulk diffusion compared with direct photodissociation. Radicals on normal sites can be formed by photodissociation or bulk diffusion, so cannot be used to measure the significance of bulk diffusion.

Table 4 shows the fraction of radicals in interstitial sites at $1.1 \times 10^5$ and $2.0 \times 10^5$ yrs. We can see that the fractions range from greater than 0.5 to very small values. The large values are most likely associated with bulk diffusion, as discussed above. In order to check if there is any time dependence, we show two different times. We can see that generally these fractions do not change much with time. The dependence of the fraction of interstitial radicals on temperature is very complicated. As the temperature increases, the mobility of interstitial species increases, which can both increase the production of interstitial radicals and eliminate interstitial radicals faster. Moreover, we saw that I(CO), which can be hydrogenated to form I(HCO), increases as temperature increases in the last subsection. Because of the above competing mechanisms, in Model 1, the fraction of all radicals in interstitial sites increases as the temperature is raised to 15 K, while, in Model 2, the fraction of $CH_2OH$ in these sites increases, the fraction of HCO does not change much, while the fraction of OH does not change at $1.1 \times 10^5$ yrs and slightly increases at $2 \times 10^5$ yrs.

We can also compare Models 1 and 2 to find out the influence of the barrier difference on the abundance of radicals. At 10 K, as we explained earlier, the abundances of all radicals do not depend on the diffusion rate before $10^4$ years. After $10^4$ yr, the abundance of OH is almost the same in both models, while the abundances of $CH_2OH$ in Model 2 are more than one order of magnitude larger than those in Model 1 at both 10 K and 15 K. The abundance of HCO in Model 2 is about 2 times as much as that in Model 1 at 10 K while at 15 K, the HCO abundance is more than one order of magnitude larger than that in Model 1. These facts can be explained by the increased mobility of interstitial species in Model 1. The influence of the barrier difference on the bulk diffusion rate is also reflected in the fraction of radicals in interstitial sites. The mobility of species on interstitial sites in Model 2 at 15 K is approximately the same as that for interstitial species at 10 K in Model 1, so we can see that the fraction in Model 2 at 15 K is very close to the fraction at 10 K in Model 1.

Finally, it is interesting to see which radical is the most abundant. The most abundant radicals are temperature dependent. For instance, in both Model 1 and Model 2 at 10 K, the most abundant radicals are $CH_3$ and $NH_2$, the abundances of which are around one monolayer (a fractional abundance with respect to hydrogen of $10^{-6}$) while at 15 K, $NH_2$, the abundance of which is more than two thirds of a monolayer, is the most abundant radical in both Model 1 and

Model 2.

### 3.3. Complex Organic Molecules

Figure 6 shows the abundances (in monolayers) of two complex organic molecules, $CH_3OCH_3$ (dimethyl ether) and $CH_3OCHO$ (methyl formate) as a function of time for Models 0, 1, and 2 at 10 K, while Table 5 lists their fractional abundances at $2 \times 10^5$ yr for both 10 K and 15 K. All the individual $CH_3OCH_3$ and $CH_3CHO$ molecules reside on normal sites. We can see that despite the fact that there are many more radicals such as $CH_2OH$ produced in Models 1 and 2 than in Model 0, the abundances of $CH_3OCH_3$ and $CH_3CHO$ in all models are very similar, which shows that interstitial chemistry plays little role in their production. These complex organic molecules are produced on the top few monolayers, so that radicals deeply buried within the ice do not contribute to their production at 10 K. The formation of complex organic molecules at 10 K cannot occur by the radical-radical mechanism of Garrod & Herbst (2006) since heavy surface radicals in this model do not move much until 30 K. Instead, $CH_3OCH_3$ is mainly produced by the following mechanism. When an H atom hops to a site in the topmost monolayer and combines with $CH_2$ to form $CH_3$, if there is a $CH_3O$ radical below the newly formed $CH_3$, they react immediately to form $CH_3OCH_3$. This is the same mechanism as that which produces $CO_2$ (Chang & Herbst 2012). Similarly, when an O atom hops into a site where there is CH residing on top of $CH_3O$, O can combine with CH first and the newly formed HCO can immediately react with $CH_3O$ to form $CH_3OCHO$. Moreover, most of the $CH_3OCH_3$ and $CH_3OCHO$ are produced before $10^5$ yr, which shows that radicals such as CH or $CH_2$ are mainly produced by hydrogenation of atomic C, whose abundance significantly drops in the gas phase with increasing time (Chang & Herbst 2012). The amounts of dimethyl ether and methy formate produced by $10^5$ yr on the ice are reasonably large but abundances of these species in cold cores can only be observed in the gas.

Table 4: Fraction of Radicals in interstitial sites

| Radicals | OH | HCO | $CH_2OH$ | OH | HCO | $CH_2OH$ |
|---|---|---|---|---|---|---|
| | 1.1(5) yr | 1.1(5) yr | 1.1(5) yr | 2.0(5) yr | 2.0(5) yr | 2.0(5) yr |
| Model 1, 10 K | 0.40 | 0.10 | 3.3(-3) | 0.36 | 7.7(-2) | 1.9(-2) |
| Model 1, 15 K | 0.58 | 0.82 | 0.50 | 0.63 | 0.83 | 0.45 |
| Model 2, 10 K | 0.36 | 6.9(-2) | 3.8(-4) | 0.33 | 5.3(-2) | 1.3(-4) |
| Model 2, 15 K | 0.36 | 6.3(-2) | 8.2(-3) | 0.43 | 5.6(-2) | 1.8(-2) |

Note. — a(-b) means $a \times 10^{-b}$.

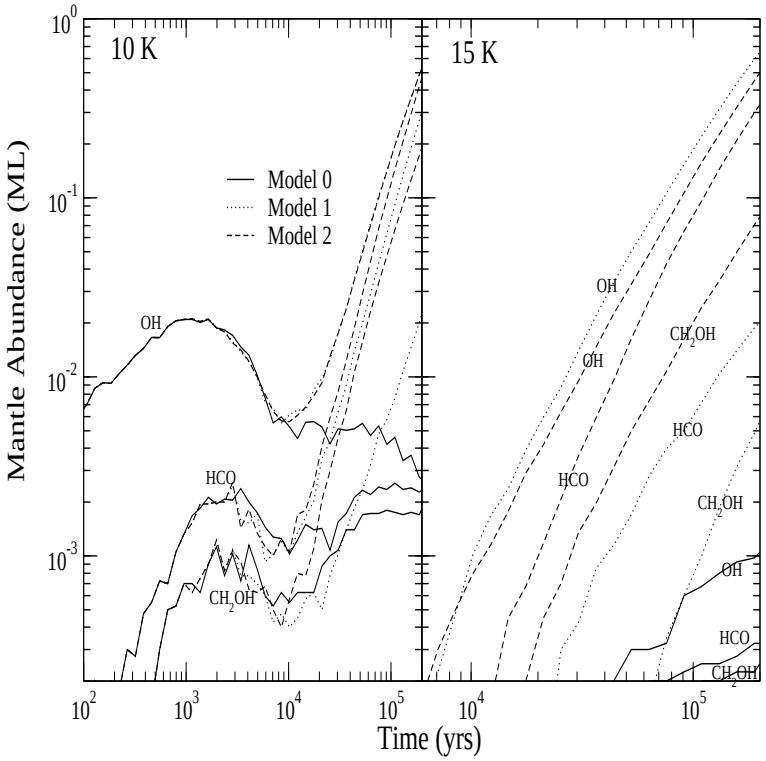


Fig. 5.— The abundance of selected radicals as a function of time for models 0, 1, and 2. Panel (a): $T = 10$ K, panel (b): $T = 15$ K.

Table 5: Fractional Abundances of Granular Complex Organic Molecules

| Species | Model 1 10 K | Model 1 15 K | Model 2 10 K | Model 2 15 K | Model 0 10 K | Model 0 15 K |
|---|---|---|---|---|---|---|
| $CH_3OCH_3$ | 1.2(-8) | 1.8(-9) | 1.2(-8) | 1.1(-9) | 1.5(-8) | 1.2(-9) |
| $CH_3OCHO$ | 3.6(-9) | 1.0(-9) | 4.1(-9) | 9.2(-10) | 3.4(-9) | 9.0(-10) |

Note. — The fractional abundances are at a time of $2 \times 10^5$ yr for Models 0, 1, 2 at different temperatures. a(-b) means a$\times 10^{-b}$.

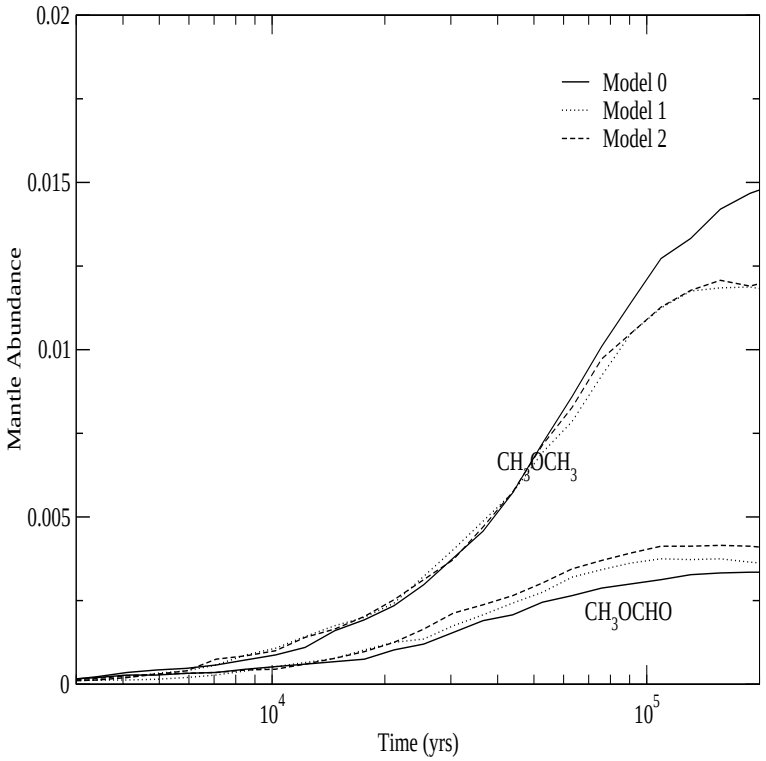


Fig. 6.— The abundance (in monolayers) of $CH_3OCH_3$ and $CH_3CHO$ as a function of time for Models 0, 1, and 2 at 10 K

## 4. Comparisons with Previous Models and Observations

The results reported in this paper are from the first simulation using a full gas-grain chemical reaction network with a microscopic Monte Carlo treatment of the grain mantle chemistry. It is interesting to compare these new results with our mantle results from a previous Monte Carlo model, in which we used a rather limited set of surface 29 surface reactions, and did not consider photodissociation or bulk diffusion (Chang & Herbst 2012). In the earlier paper, a comparison with older rate-equation models was also made. Table 6 shows a comparison between our current results for CO, $CO_2$, $CH_3OH$, and $CH_4$ ices and those of a previous Monte Carlo model (Model 3) with the same parameters as our current Model 0 at 10 K so that only the number of grain mantle reactions differs. We also make a thorough comparison with observational results of a compendium of sources in front of background stars, high-mass YSOs and low-mass YSOs (Öberg et al. 2011a), adding $NH_3$ to the list of molecules. The abundances are listed as percentages of the water ice abundance. The results from Models 0, 1, and 2 are very similar, so that bulk diffusion and photodissociation are clearly not critical for the species shown.

The median observed water fractional abundance, about $5\times10^{-5}$ (Gibb et al. 2004; Pontoppidan et al. 2004; Boogert & Ehrenfreund 2004; Öberg et al. 2011a), is in excellent agreement with all our current simulations at $2 \times 10^5$ yr regardless of photon penetration or temperature (10 K or 15 K). The agreement between current Model 0 (10 K) and the older Model 3 (10 K) is very good for CO, $CO_2$, and $CH_3OH$, while the older model predicts somewhat more methane. Regarding observations, the results of our model simulations are in reasonable agreement with the summary of observational results of Öberg et al. (2011a), especially at 15 K, although our results for $CO_2$ are a factor of a few too low except for high mass stars, and our results for ammonia are high by a factor 3-5.

In addition to total abundances, we can look at the abundances of major ice species with respect to monolayer. Observational results show that CO may exist in two distinct phases on grain surfaces formed at different times (Tielens et al. 1991; Öberg et al. 2011a), and a careful discussion with respect to our earlier Monte Carlo calculations can be found in Chang & Herbst (2012). The polar phase, produced early in the mantle evolution, is $H_2O$-dominated, but also possesses abundant $CO_2$. The non-polar phase, produced later, is CO-dominated with some conversion to formaldehyde and methanol. Our simulations $2 \times 10^5$ yr do show a slight trend of more abundant CO and methanol at outer layers caused by the increased abundance of gas phase CO and decreased abundance of atomic O at later times. However, even at the end of our simulation, $H_2O$ is always the most abundant species in each layer, as can be seen in Figure 4. This dominance cannot be explained by the "short" evolution in our simulation because even with a three-phase rate equation model, which can be run to much longer times, $H_2O$ is always the most abundant species at each layer (Garrod & Pauly 2011). One possible explanation is that grains can undergo some thermal processing, which induces segregation or distillation of $CO_2$ or CO (Öberg et al. 2009c; Pontoppidan et al. 2008). In our simulations, CO molecules are able to move around within the ice mantle, but they cannot evaporate between 15 K and 20 K so they may be able to diffuse gradually to the top layers and form CO-rich layers. Thus, the position of each molecule in the ice mantle may not be the actual positions where they were formed. However, a more complicated model with

Table 6. Comparison of Observational and Ice Abundances By Different Models at $2 \times 10^5$ Yr

| | CO | $CO_2$ | $CH_3OH$ | $CH_4$ | $NH_3$ |
|---|---|---|---|---|---|
| Our New MC Models | | | | | |
| Model 1, 10 K | 15.3 | 9.1 | 4.7 | 11.0 | 20.9 |
| Model 1, 15 K | 30.8 | 11.3 | 3.8 | 5.8 | 16.1 |
| Model 2, 10 K | 14.9 | 9.1 | 4.7 | 11.1 | 20.9 |
| Model 2, 15 K | 30.5 | 11.3 | 3.8 | 5.3 | 15.9 |
| Model 0, 10 K | 13.7 | 10.0 | 6.3 | 13.7 | 23.2 |
| Model 0, 15 K | 29.6 | 12.2 | 4.7 | 6.1 | 17.2 |
| Our Previous MC Model | | | | | |
| Old Model 3, 10 K | 10.5 | 11.3 | 9.8 | 21.2 | – |
| Observations | | | | | |
| Toward Low Mass Stars | 29 | 29 | 3 | 5 | 5 |
| Toward High Mass Stars | 13 | 13 | 4 | 2 | 5 |
| Toward Background Stars | 31 | 38 | 4 | | |

Note. — The abundances of major ice mantle components are percentages with respect to the water ice. a(-b) means $a \times 10^{-b}$.

segregation or distillation coupled with the full gas-grain network simulation is not the purpose of this work.

A major feature in the calculations reported here is the higher abundances of radicals with bulk diffusion and photon penetration included in Models 1 and 2. Moreover, it is photon penetration that generates bulk diffusing species deeply buried within the ice in our simulation.In the work by Garrod (2013a) photodissociation reactions are allowed to occur at equal rates within ice mantle, however, the abundance of radicals was not reported in Garrod (2013a). A high abundance of radicals was obtained by photodissociation of bulk ice in experiments of Greenberg and colleagues (Schutte & Greenberg 1991) and shown to lead to explosions when warmed up. Although the GRAINOBLE model (Taquet et al. 2012) also produces a significant abundance of radicals, the mechanism to form radicals is very different from that in our approach. In particular, the radicals formed with the GRAINOBLE model simulation are actually normal species that react with other species, which is equivalent to that in our earlier work (Chang et al. 2007), where we also produced many radicals. However, with the introduction of the swap of H atoms and other species in the top 4 monolayers (Chang & Herbst 2012; Cuppen et al. 2009), these radicals are almost completely destroyed, as occurs in Model 0. The radicals formed in Model 1 are, on the other hand, almost all formed by photodissociation of stable species deeply buried in the ice mantle and by reaction with photodissociation products. We can qualitatively compare our results with those of the molecular dynamics (MD) calculation by Andersson & van Dishoeck (2008). In this calculation, the products of photodissociated $H_2O$ at the sixth monolayer, covered by 5 monolayers of water ice, can recombine again with a probability of 0.4 so almost 60% of the photodissociated $H_2O$ molecules are frozen in the ice mantle in the form of OH radicals or water, formed from OH + H. This qualitatively agrees with our large abundance of radicals after introducing photon penetration.

The $CH_3O$ radical, which is contained in our models, has been recently detected in the cold core B1-b with a low fractional abundance of $4.7 \times 10^{-12}$ in gas phase (Cernicharo et al. 2012). Although the calculated granular $CH_3O$ fractional abundance in Model 1 at 10 K is more than $10^{-8}$, because we do not include any very efficient non-thermal desorption mechanisms, the gas-phase $CH_3O$ radical abundance remains very low in our simulation. It is not clear if we can produce the gas phase abundance of $CH_3O$ radical with reactive desorption, which can efficiently desorb surface species.

Another new feature of our results is the prediction that complex organic molecules such as $CH_3OCHO$ and $CH_3OCH_3$ can be formed on ice mantles at temperatures as low as 10 K with fractional abundances of a few $\times 10^{-8}$ for $CH_3OCH_3$ and a few $\times 10^{-9}$ for $CH_3OCHO$ at $2 \times 10^5$ yr. Recent observations (Bacmann et al. 2012) show that the fractional abundance of these two complex organic molecules in the gas phase in cold cores is about a few $10^{-10}$. However, all $CH_3OCHO$ or $CHO_3CH_3$ molecules in our models only exist on grain surfaces because there is no efficient desoption mechanism included in our models. If 10% of these two complex organic molecules can be desorbed and not destroyed in the gas phase, their gaseous fractional abundance in our models will agree well with observations. However, because these two molecules can be destroyed in the gas phase, it is not clear if we can predict the observed abundance of these two complex organic

molecules when an efficient desorption mechanism such as reactive desorption (Vasyunin & Herbst 2013a) is included.

## 5. Conclusions and Discussion

Despite the fact that the microscopic-macroscopic Monte Carlo method is exceedingly computationally demanding, we have successfully simulated the gas-grain chemistry of a cold dense core with a gas-grain reaction network containing $\approx 300$ surface reactions. Our simulations, which follow the chemical evolution for $2 \times 10^5$ yr, represent a significant advance compared with our earlier microscopic Monte Carlo simulations, with fewer than 30 surface reactions (Chang & Herbst 2012). The new simulations have been made possible by the use of an improved and more efficient algorithm, in which the species in the simulations are divided into three groups depending on the strength of their binding energy to the grain. With this algorithm, we are able to follow additional processes involving the chemistry that occur in the bulk of the ice mantle. These processes include photon penetration and molecular dissociation caused by the penetrating photons. Moreover, we are also able to follow a bulk chemistry occurring on interstitial sites located between sites of normal binding energy and maintained by photo-production of radicals. We have focused the discussion in this paper on grain mantle species because species heavier than hydrogen and helium cannot efficiently desorb at temperatures below 15 K. The result is that the abundances of the gas-phase species in our three models are similar to those in two-phase models, where no distinction is made between surface and bulk mantle. In a subsequent paper, we will include non-thermal reactive desorption so that all species on the grain surface can efficiently desorb; the abundances of gas phase species will then be more tightly coupled with the chemical composition of the ice mantle.

Our simulations show that the abundances of major stable ice species are not affected appreciably by photon penetration; thus, the simulation results concerning stable major species in our previous study of cold cores are still valid. Moreover, the results of both our past and current models agree reasonably well with observations of the abundance of major species for sources toward high mass YSOs, low mass YSOs, and background stars. The major difference between the current work and past work has to do with the calculated granular abundances of radicals. Formed mainly by photodissociation, the radicals can be enhanced in abundance by up to two orders of magnitude over models without this process in the bulk. The high abundance of radicals qualitatively agrees with recent studies using rate equations (Taquet et al. 2012) or molecular dynamical simulations (Andersson & van Dishoeck 2008). The bulk diffusion of light species formed by photodissociation can also lead to the formation of other radicals by interstitial reactions, a process never before included in previous models, although a similar model with pores has been reported (Kalvans & Shmeld 2013). With all the radicals trapped within ice mantles, especially at 10 K, chains of chemical reactions can occur when thermal processing of ice mantles occurs and the radicals are able to move more freely. In this instance, explosions might even occur (Rawlings et al. 2013). This more complicated scenario will be included in a future study.

Our simulations also show that the chemistry occurring on and in grain mantles might be far more complex than it seems to be, especially when we treat ice mantle layers other than the topmost layer as a partially chemically active phase, and bulk diffusion of species within the ice mantle. Indeed, the ice mantle, especially deep inside it, is a particularly ideal location for radical-radical association reactions because radicals will not find many other species with which to react. Other types of reactive species accreting from the gas will not approach deeply buried radicals, and in addition, there are few atoms available deep in the bulk. So the temperature range where radical-radical association reaction dominate should be much broader than when these reactions happen on the topmost layers where radicals can be easily depleted by the large amount of species accreting from the gas phase and, in addition, these radicals can evaporate when the temperature is high enough, as occurs in later stages. Moreover, the fact that complex organic molecules such as $CH_3OCH_3$ can be formed on the topmost ice layers when the temperature is as low as 10 K further illustrates the major difference between reactions on the grain surface and those in the gas phase. Unlike the gas phase, because species are packed densely in ice mantles, three-body reactions such as the chain reaction mechanism occur frequently within the ice.

It should be emphasized that interstitial bulk diffusion, which describes how molecules diffuse within a crystal lattice, is a realistic physical process, and might be the dominant bulk process at temperatures as low as 10 K. Moreover, when a molecule is photodissociated within the bulk, if potential minima around this molecule are normally occupied, some products of the photodissociation reaction have to stay in interstitial sites. Thus, we must take into account interstitial sites in modeling and simulation if we allow species deeply buried within ice mantle to be photodissociated. However, it remains a large challenge to calculate the location of interstitial sites if we want to adopt a more rigorous off-lattice microscopic Monte Carlo approach (Garrod 2013b). Based on such a simulation, the ice formed on a grain surface is non-porous if the gas density pertains to typical dark clouds ($n_H = 2 \times 10^4\ cm^{-3}$); however, an ice mantle can be porous with a gas phase density much higher than that of typical dark clouds ($n_H \geq 2 \times 10^5\ cm^{-3}$) (Garrod 2013b). If an ice mantle formed on a grain surface is porous, our interstitial bulk diffusion model has to be modified.

The details that can be obtained with a microscopic model of the grain chemistry should allow us to understand much better the different environments, both polar and non-polar, on grain mantles. But to understand these environments better than we currently do, we may have to add more complex physical processes such as segregation, or distillation dynamics, into the simulation. These processes may change our results significantly because light species such as CO may tend to be more abundant in outer layers with segregation or distillation dynamics included than in our current models. Although it would be worthwhile to study the further details of mantle chemistry, the unified microscopic-macroscopic Monte Carlo simulation has a serious problem: it takes too much simulation time. For instance, at 15 K, Models 1 and 2 take more than 8 days to simulate the evolution of the system through $2 \times 10^5$ years with our Dell Presion T7500n workstation. Because of the high computational cost, we have not yet been able to simulate the chemistry occurring during the warm-up phase of stellar evolution, which should be very interesting. Besides this very

serious problem, other issues remain outstanding. For example, most of the surface reactions in our network with experimentally determined activation energy barriers have not been fitted by the competition mechanism in our simulation (Herbst & Millar 2008), with the exception of CO + H and $H_2CO$ + H, so it is not clear if we can still use these barriers, especially if determined from gas-phase reactions, for simulation by our approach. Finally, whether we use a microscopic or even a macroscopic Monte Carlo simulation for the grain chemistry, reactions involving $H_2$ on and in the grain mantle cannot be treated correctly because the rapid accretion and desorption of $H_2$ make Monte Carlo simulations currently not feasible. Some approximations and/or more powerful computers have to be introduced to solve this problem.

We are thankful to the referee for suggestions for revision that have improved this paper. EH wishes to acknowledge the support of the National Science Foundation for his astrochemistry program. He also acknowledges support from the NASA Exobiology and Evolutionary Biology program through a subcontract from Rensselaer Polytechnic Institute. We thank Anton I. Vasyunin for helpful discussions and allowing us to use his rate equation codes and network.

## REFERENCES

Akiyama, A., Hosoi, T., Ishihara, I., Matsumoto, S., & Niimi, T. 1987, IEEE Trans. on Comp. Aided Design CAD-6, 185

Andersson, S., & van Dishoeck, E. F. 2008, A&A, 491, 907

Bacmann, A., Taquet, V., Faure, A., Kahane, C., & Ceccarelli, C. 2012, A&A, 541, L12

Biham, O., Furman, I., Pirronello, V., & Vidali, G. 2001, ApJ, 553, 595

Boogert, A. C. A., & Ehrenfreund, P. 2004, in Astrophysics of Dust, ASP Conference Series, Vol. 309, ed. A. N.Witt, G. C. Clayton, B. T. Draine, p. 547

Caselli, P., Hasegawa, T. I., & Herbst, E. 1998, ApJ, 495, 309

Cernicharo, J., Marcelino, N., Roueff, E., et al. 2012, ApJL, 759, L43

Chang, Q., & Herbst, E. 2012, ApJ, 759, 147

Chang, Q., Cuppen, H. M., & Herbst, E. 2005, A&A, 434, 599

Chang, Q., Cuppen, H. M., & Herbst, E. 2007, A&A, 469, 973

Charnley, S. B. 1998, ApJ, 509, L121

Charnley, S. B., & Rodgers, S. D. 2009, in ASP Conf. Ser. 420, Bioastronomy 2007: Molecules, Microbes and Extraterrestrial Life, ed. K. Meech et al. (San Francisco, CA: ASP), 29

Congiu, E., et al. 2012, ApJ, 750: L12(1-4)

Cuppen, H. M. & Herbst, E. 2005, MNRAS, 361, 565

Cuppen, H. M., van Dishoeck, E. F., Herbst, E., & Tielens, A. G. G. M. 2009, A&A, 508, 275

Du, F. & Parise, B. 2011, A&A, 530, A131

Fayolle, E. C., Öberg, K., Cuppen, H. M., Visser, R., & Linnartz, H. 2011, A&A, 529, A74

Fuchs, G. W., Cuppen, H. M., Ioppolo, S., Romanzin, C., Bisschop, S. E., Andersson, S., van Dishoeck, E. F., & Linnartz, H 2009, A&A, 505. 629

Garrod, R. 2008, A&A, 491, 239

Garrod, R. 2013a, ApJ, 765, 60

Garrod, R. 2013b, ApJ, 778, 158

Garrod, R., & Herbst, E. 2006, A&A, 457, 927

Garrod, R., & Pauly, T. 2011, ApJ, 735, 15

Garrod, R. T., Vasyunin, A. I., Semenov, D. A., Wiebe, D. S., & Henning, Th. 2009, ApJ, 700, L43

Gibb, E. L., Whittet, D.C. B., Boogert, A. C. A., & Tielens, A. G. G. M. 2004, ApJS, 151, 35

Gibson, M. A., & Bruck, J. 2000, J. Phys. Chem., 104, 1876

Gillespie, D. T., 1976, J. Comp. Phys., 22, 403

Green, N. J. B., Toniazzo, T., Pilling, M. J., Ruffle, D. P., Bell, N., & Hartquist T. W. 2001, A&A, 375, 1111

Hasegawa, T. I., & Herbst, E., 1993, MNRAS, 263, 589

Hasegawa, T. I., Herbst, E., & Leung, C. M.1992, ApJS, 82, 167

Herbst, E., & Millar, T. J. 2008, in Low Temperatures and Cold Molecules, ed. I. W. M. Smith (London, Imperial College Press), p. 1

Herbst, E., & Shematovich, V. I. 2003, Ap&SS, 285, 725

Jenniskens, P., Blake, D. F., Wilson, M. A., & Pohorille, A. 1995, ApJ, 455, 389

Kalvans, J., & Shmeld, I. 2013, A&A, 554, 111

Lipshtat, A., & Biham, O. 2003, A&A, 400, 585

Öberg, K., Boogert, A. C. Adwin , Pontoppidan, K. M., Van Den Broek, S., van Dishoeck, E. F., Bottinelli, S., Blake, G. A., & Evans II, N. J., 2011a , ApJ, 740, 109

Öberg, K., Fayolle, E. C., Cuppen, H. M., van Dishoeck, E. F., & Linnartz, H. 2009a, A&A, 505, 183

Öberg, K., Fuchs, G. W., Awad, Z., Fraser, H. J., Schlemmer, S., van Dishoeck, E. F., & Linnartz, H., 2007, ApJ, 662, L23

Öberg, K., Linnartz, H., Visser, R., & van Dishoeck, E. F. 2009b, ApJ, 693, 1209

Öberg, K., van Dishoeck, E. F., & Linnartz, H., 2009c, A&A, 496, 281

Pickles, J. B., & Williams, D. A. 1977, Ap&SS, 52, 443

Pontoppidan, K. M., Boogert, A. c. A., Fraser, H. J., van Dishoeck, E. F., Balke, G. A., Lahuis, F., Öberg, K., Evans, N. J., & Salyk, C. 2008, ApJ, 678, 1005

Pontoppidan, K. M., van Dishoeck, E. F., & Dartois, E. 2004, A&A, 426, 925

Rawlings, J. M. C., Williams, D. A., Viti, S., Cecchi-Pestellini, C., Duley, W. W. 2013, MNRAS, 430, 264

Schutte, W. A., & Greenberg, J. M. 1991, A&A, 244, 190

Semenov, D., Hersant, F., Wakelam, V., Dutrey, A., Chapillon, E., Guilloteau, S., Henning, T. Launhardt, R., Piétu, V., & Schreyer K. 2010, A&A, 522, A42

Shen, C. J., Greenberg, J. M., Schutte, W.A., & van Dishoeck, E.F. 2004, A&A, 415, 203

Smith, R. G., Charnley, S. B., Pendleton, Y. J., Wright, C. M., Maldoni, M. M., & Robinson, G. 2011, ApJ, 743, 131

Stantcheva, T., & Herbst, E. 2004, A&A, 423, 241

Taquet, V., Ceccarelli, C., & Kahane, C. 2012 A&A, 538, A42

Tielens, A. G. G. M, & Charnley, S. B. 1997, Origins Life Evol. B., 27, 23

Tielens, A. G. G. M., Tokunaga, A. T., Geballe, T. R., & Baas, F. 1991, ApJ, 381, 181

Vasyunin, A. I., & Herbst, E. 2013a, ApJ, 769, 34

Vasyunin, A. I., & Herbst, E. 2013b, ApJ, 762, 86

Vasyunin, A. I., Semenov, D. A., Wiebe, D. S., & Henning, T. 2009, ApJ, 691, 1459

Watanabe, N., & Kouchi, A. 2002, ApJ, 571, L173

This preprint was prepared with the AAS LaTeX macros v5.2.